Dynamics of the Lignin Glass Transition

Journal:	*Physical Chemistry Chemical Physics*
Manuscript ID	CP-ART-05-2018-003144.R1
Article Type:	Paper
Date Submitted by the Author:	12-Jul-2018
Complete List of Authors:	VURAL, DERYA; Giresun University, Physics Department Smith, Jeremy; Oak Ridge National Laboratory, UT/ORNL Center for Molecular Biophysics Petridis, Loukas; Oak Ridge National Laboratory, Center for Molecular Biophyscis

Journal Name

ARTICLE TYPE

Cite this: DOI: 10.1039/xxxxxxxxxx

Received Date
Accepted Date

DOI: 10.1039/xxxxxxxxxx

www.rsc.org/journalname

Dynamics of the Lignin Glass Transition†

Derya Vural,*[a,b,c] Jeremy C. Smith,[a,c] and Loukas Petridis[a,c]

The dynamics of lignin, a complex and heterogeneous major plant cell-wall macromolecule, is of both fundamental and practical importance. Lignin is typically heated to temperatures above its glass transition to facilitate its industrial processing. We performed molecular dynamics simulations to investigate the segmental (α) relaxation of lignin, the dynamical process that gives rise to the glass transition. It is found that lignin dynamics involves mainly internal motions below T_g, while segmental inter-molecular motions are activated above T_g. The segments whose mobility is enhanced above T_g consist of 3-5 lignin monomeric units. The temperature dependence of the lignin segmental relaxation time changes from Arrhenius below T_g to Vogel-Fulcher-Tamman above T_g. This change in temperature dependence is determined by the underlying energy landscape being restricted below T_g but exhibiting multiple minima above T_g. The Q-dependence of the relaxation time is found to obey a power-law up to Q_{max}, indicative of sub-diffusive motion of lignin above T_g. Temperature and hydration affect the segmental relaxation similarly. Increasing hydration or temperature leads to: (1) the α process starting earlier, i.e. the beta process becomes shortened (2) Q_{max} decreasing, i.e. the lengthscale above which subdiffusion is observed increases (3) the number of monomers constituting a segment increasing, i.e. the motions that lead to the glass transition become more collective. The above findings provide a molecular-level understanding of the technologically important segmental motions of lignin and demonstrate that, despite the heterogeneous and complex structure of lignin, its segmental dynamics can be described by concepts developed for chemically homogeneous polymers.

Introduction

Lignocellulosic biomass is an abundant and renewable source material for the production of biofuels, thermoplastics and synthetic fibers[1–4]. Biomass is made of lignin, cellulose and hemicellulose polymers. Lignin, accounting for 15-25% of the dry weight of woody plant, is used for the production of carbon fibers, plastics, colloidal particles and films[5–11], but it also poses serious challenges for biomass utilization. Thermal pretreatment is commonly used to remove lignin from biomass, which improves the production of biofuels and other bioproducts[12–14]. During thermal pretreatment, structural and dynamical changes such as the delocalization of lignin are observed in biomass due to the applied high temperature[1–3].

Generally, the dynamics of polymers is different at temperatures below and above the glass transition temperature, T_g[15,16]. At $T < T_g$, a polymer is in a glassy state and its atoms exhibit localized dynamics, also called the β relaxation process. At $T > T_g$, the polymer dynamics crosser over to the α relaxation process, in which a polymer becomes less viscous and flows because of activated segmental motions. The thermodynamic glass transition temperature is usually determined by differential scanning calorimetry (DSC)[17,18] or specific volume measurement[19–21]. T_g of lignin lies in a broad temperature range, $110-150\,C^{\circ}$, the value depending on the biomass source, heating rate and molecular weight[4,17,18,22–26].

Glass-forming polymers have been studied experimentally and theoretically[16,27–35]. Segmental motions, in which many monomers move collectively, are recognized to play a critical role in the glass transition. Lignin, however, has a complex molecular structure: it is made of a random sequence of three types of monomers (often called "units") connected by numerous inter-unit linkages. Furthermore, lignin molecules are believed to have different primary structures in plants, so that one lignin molecule may be different to another. In some respects, lignin should not be considered as a polymer due to its irregular primary structure.

[a] UT/ORNL Center for Molecular Biophysics, Oak Ridge National Laboratory, P.O. Box 2008, Tennessee 37831
[b] Department of Physics, Giresun University, Giresun, 28200, Turkey Fax: +90 454 310 1477; Tel: +90 454 310 1400 (4062); E-mail: derya.vural@giresun.edu.tr
[c] Department of Biochemistry and Cellular and Molecular Biology, University of Tennessee, Knoxville, TN 37996, USA.

† Electronic Supplementary Information (ESI) available: [details of any supplementary information available should be included here]. See DOI: 10.1039/b000000x/

It is therefore important to establish whether the description obtained for chemically simple glass-forming polymers holds for the significantly more heterogeneous and complex lignin.

Here, we investigate the relaxation processes of lignin by using molecular dynamics (MD) simulations. We analyze 0.05 and 0.25 hydration levels (g water per g lignin), which correspond to a typical powder form of lignin isolated from biomass, and lignin in its native secondary plant cell walls, respectively. The motions of atoms giving rise to the dynamical processes of lignin are revealed by principal component analysis. The motions are decomposed into intra- and inter-molecular contributions, the latter being activated above T_g. The temperature dependence of the lignin relaxation time is found to transition from Arrhenius below T_g to non-Arrhenius above T_g, similar to glass-forming polymers. The simulations furnish an atomic-level description of the segmental motions of lignin that are critical to its thermal processing.

Methods

Model Generation

Nuclear magnetic resonance information on the average chemical composition of vanillia stem lignin[36], which has been extensively characterized, was used to construct models of individual lignin molecules. Vanillia lignins are composed of guaiacyl (G) and syringly (S) units, bonded by various linkages. We constructed structural models of four different lignin polymers that approximately match 2D-NMR experimental data[36]: the polymers comprised 16 G units and 6 S units, with a molecular weight of 5 kDa, and average linkage composition of $\beta-O-4'$ 76%, $\beta-5$ 19% and $\beta-\beta$ 5%. The primary sequence of each lignin can be found in Tables S1-S4 of the Supporting information (S.I.).

MD Simulation

The simulation systems contained randomly oriented four lignin polymers packed in a box of dimensions 35 Å × 38 Å × 30 Å. The lignin polymers were solvated at two different hydration levels, h = 0.05 and 0.25 g_{water}/g_{lignin}, corresponding to 56 and 276 water molecules, respectively. The box was replicated using periodic boundary conditions. NAMD[37] was used to perform the simulations with a time step of 2 fs for bonded and short-range non-bonded interactions, and 4 fs for long-range electrostatic interactions. The TIP3P water model[38] and the CHARMM force field for lignin[39] were employed. The Particle Mesh Ewald method[40] was used to model the electrostatic interactions with a grid spacing of 1 Å and a force-switching function to smoothly transition the Leonard Jones interaction to zero over the range of 10 - 11 Å. The neighbor search was performed every 20 steps with a pair-list distance of 12.5 Å. The cutoff distance for the nearest neighbour search was 11 Å. The temperature and pressure were maintained by using the Langevin dynamics[41] and the Nose-Hoover Langevin piston[42] algorithms, respectively. A damping coefficient of 5 ps^{-1} was used for the Langevin dynamics algorithm. The Nose-Hoover Langevin piston algorithm employed a piston oscillation period of 200 fs and a piston damping decay time of 100 fs.

Each system was simulated for 150 ns at 1 bar and 34 temperatures from 150 to 480 K in 10 K increments. The coordinates were saved every 1 ps. Data from the last 75 ns were analysed at each temperature. All calculations were performed on the Edison and Hopper supercomputers at NERSC.

Analysis

To characterize the lignin dynamics we calculated a Fourier space- and time-dependent correlation function, the incoherent intermediate scattering function (ISF),

$$I(Q,t) = \frac{1}{N}\sum_{i=1}^{N} b_i^2 \langle \exp[-i\mathbf{Q}.(\mathbf{r}_i(t)-\mathbf{r}_i(0))]\rangle. \quad (1)$$

where $\mathbf{r}_i(t)$ is the position of atom i at the reference time t, N is the number of atoms, $\mathbf{Q}$ is the scattering vector, its magnitude being $Q=|\mathbf{Q}|$, b_i is the incohorent scattering length of nucleus i and the brackets denote ensemble and orientation averages. b of hydrogen is almost 20 times larger than for other atoms. $I(Q,t)$ can be determined in neutron scattering experiments, a particularly useful technique for probing atomic motions in biomolecules. To mimic a neutron scattering experiment performed in D_2O, the exchangeable hydrogen atoms in the lignin molecules were assigned the scattering length of deuterium. A large contribution to $I(Q,t)$ thus comes from the non-exchangeable hydrogen atoms in lignin molecules. $I(Q,t)$ for lignin was calculated from the MD using SASSENA[43]. Finite size effects lead to motions with wavelengths longer than the box size being suppressed. Here, with a periodic box size of 37 Å, these motions correspond to $\sim 2\pi/(37\text{ Å}) \sim 0.17$ Å^{-1}. We examine motions corresponding to $Q > 0.2$ Å^{-1}, which are less likely to be influenced by finite size effects.

The average atomic mean square displacement (MSD) was directly calculated from the MD simulations,

$$\langle r^2\rangle = \frac{1}{N}\sum_{i=1}^{N}\langle(\mathbf{r}_i(t)-\mathbf{r}_i(0)^2)\rangle \quad (2)$$

where $\langle . \rangle$ represents an ensemble average, $\mathbf{r}_i(t)$ is the position of atom i at reference time t, and N is the number of atoms.

Principal component analysis (PCA)[44,45] was used to investigate the collective motions of molecules by diagonalizing the covariance matrix,

$$\mathrm{Cov}(i,j) = \langle(\mathbf{r}_i - \langle\mathbf{r}_i\rangle)\cdot(\mathbf{r}_j - \langle\mathbf{r}_j\rangle)\rangle, \quad (3)$$

where $\mathbf{r}_i$ and $\langle\mathbf{r}_i\rangle$ are the coordinates and the average coordinates of atom i, to determine a set of eigenvectors and corresponding eigenvalues, which together define the principal component modes. The eigenvalue λ_i determines the amplitude of the ith mode. The first eigenvectors give the direction of the major motions in the system. Here, PCA was performed with and without eliminating relative motions between lignin molecules, using all 580 atoms of each lignin molecule, yielding 3×580=1740 components.

Results

To determine T_g, we calculated the specific volume (inverse density) of the simulation system at each temperature. The temperature dependence of the specific volume changes significantly at

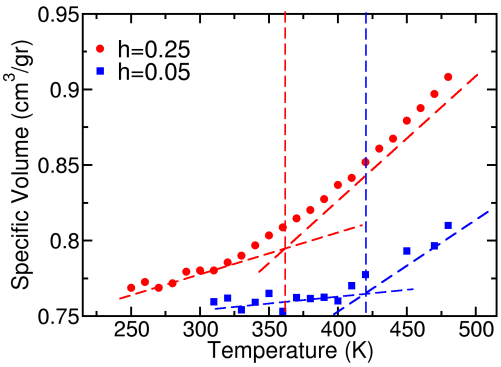

Fig. 1 Specific volume versus temperature for $h = 0.05$ (blue solid squares) and $h = 0.25$ (red solid circles) g_{water}/g_{lignin}. The dashed lines are guides to the eye.

T_g, which is found to be around 400 K for the 5% hydrated sample and around 350 K and, smaller for the 25% hydrated sample (Fig. 1). The glass transition temperature thus decreases with increasing hydration. This break in the rate of change of the specific volume with temperature is associated with a change in dynamics, which we investigate below. At $T < T_g$, lignin displays only local dynamics, whereas segmental motions are activated above T_g and the system can be rearranged to pack efficiently upon cooling.

Principal Component Analysis

We performed PCA on single lignin molecules to determine the dominant motions above and below T_g. The highest eigenvalue PCA modes typically have a high degree of collectivity, describing dynamics involving both inter- and intra-molecular motions, and capture the largest fluctuations. For example, the first principal component accounts for 58% and 35% of the total variance for the 5% and 25% hydrated samples, respectively (Fig. S-1). At 300 K, in the first PC, for both hydration levels, atoms belonging to different monomers move largely independently. However, at 480 K the fluctuations become increasingly segmental: atoms spanning multiple monomers move together (Fig. 2). This is consistent with correlation of monomers motions becoming stronger at 480 K (Fig. S-2). Correlations between atomic displacement vectors indicate that the segments comprise about 3 and 5 monomers at h = 0.05 and 0.25, respectively (Fig. S-3). Thus, at a given temperature, hydration increases the size of a segment.

The total lignin dynamics includes internal intra-molecular motions and intermolecular motions in which whole molecules move relative to each other. To evaluate how much internal motions contribute to the different principal modes, we took the dot product between the PCA eigenvectors calculated in two ways: using the full trajectories of each atom ("total") and after removing the whole-molecule translation and rotation ("internal", see Fig. 3). Strong correlation between the eigenvectors of internal and total motions indicates that internal motions dominate. Weaker correlation implies intermolecular motions have been activated. With

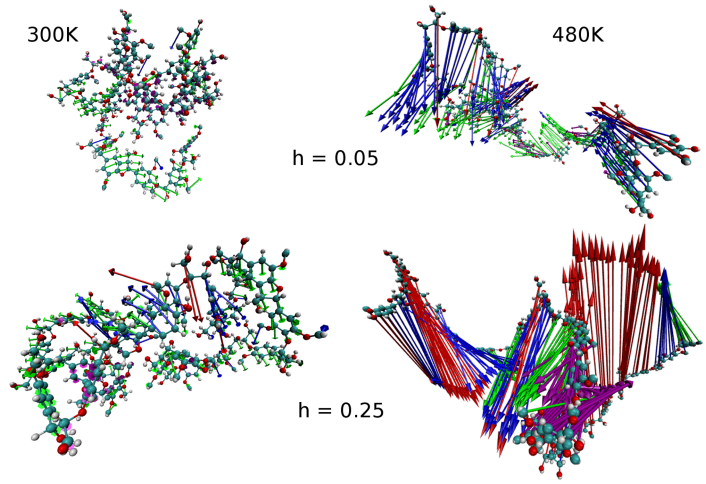

Fig. 2 The motions of atoms in a lignin molecule for the first PC eigenvector at (left-hand-side(LHS)) 300 and (rigt-hand-side(RHS)) 480 K [(top) 0.05 and (bottom)0.25 hydrated sample]. This data includes the contribution of the internal and relative motions. Red arrows represent the largest contribution to the first PCA mode.

increasing hydration and temperature, the correlation becomes poorer, and thus the contribution of the inter-molecular motions is enhanced.

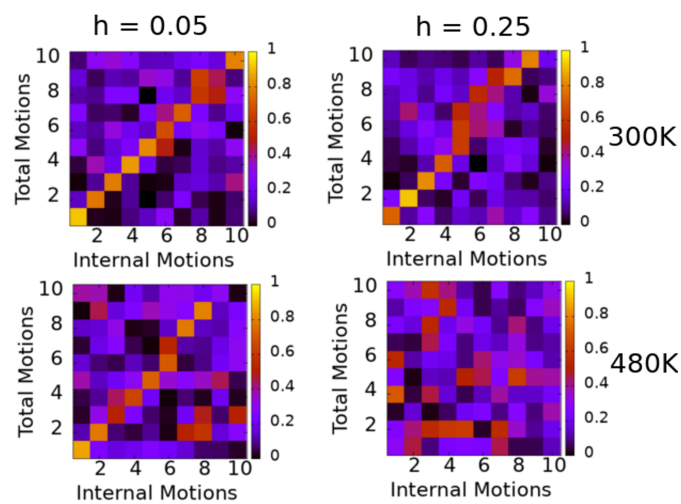

Fig. 3 Correlation between internal and total motions at (top) 300 and (bottom) 480 K for (LHS) $h = 0.05$ and (RHS) $h = 0.25$ g_{water}/g_{lignin}.

β and α relaxation processes

To charecterize the length and time scale dependence of motions in lignin, we calculated the incoherent ISF $I(Q,t)$ in Eq. (1) for Q values between 0.2 and 2 Å^{-1}. We examine here two processes in lignin dynamics, the β and α relaxations[46–49]. Two steps are observed in $I(Q,t)$ at temperatures below T_g (Fig. 4a). In the first ps step, $I(Q,t)$ decays to a near plateau, this decay representing the β relaxation and involving local, intra-molecular motions[50]. $I(Q,t)$ decays away from the plateau in a second ns step, signaling

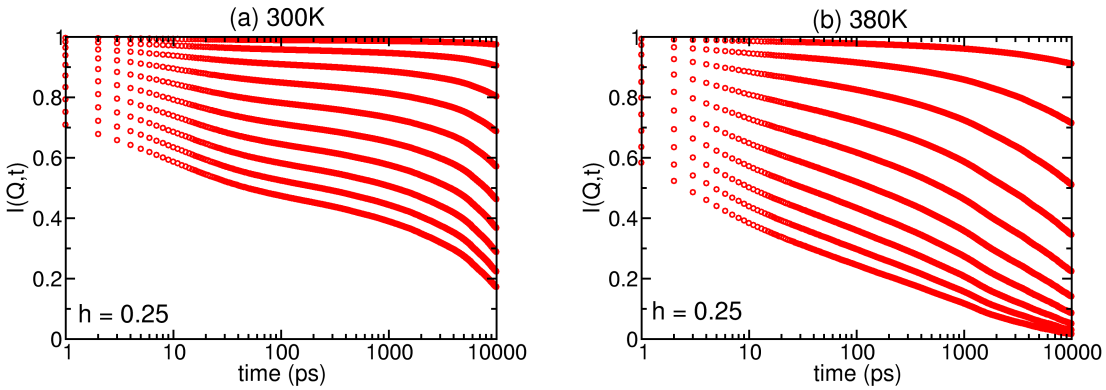

Fig. 4 The intermediate scattering function $I(Q,t)$ versus time for $h = 0.25\ g_{water}/g_{lignin}$ at (a) 300 and (b) 380 K. From top to bottom, Q values are 0.2, 0.4, 0.6, 0.8, 1.0, 1.2, 1.4, 1.6, 1.8 and 2.0 Å^{-1}.

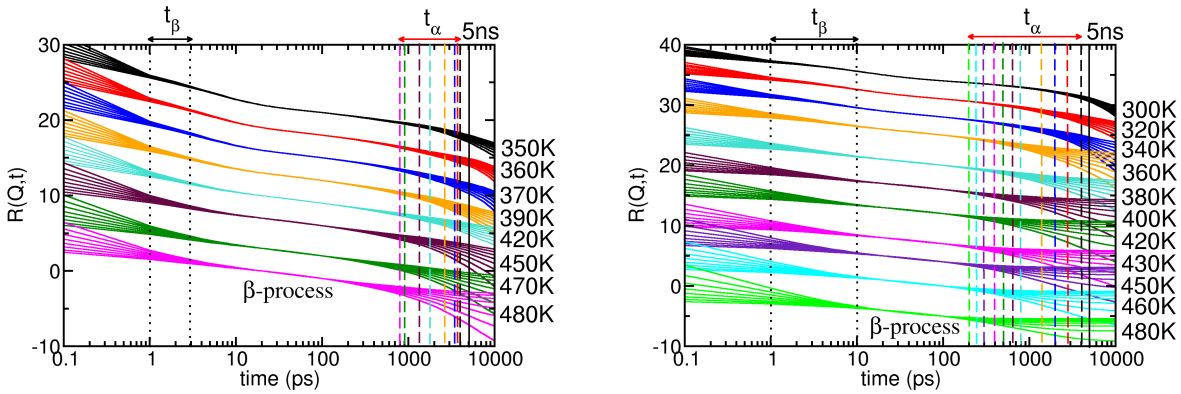

Fig. 5 $R(Q,t)$ defined in Eq. (5), versus time for (LHS) $h = 0.05$ and (RHS) $h = 0.25\ g_{water}/g_{lignin}$. $t' = 100$ and $t'' = 20$ ps are used. At each temperature, plotted in a different colour, the 8 lines represent Q values between 0.6 and 2 Å^{-1}. The dotted black line represents the approximate time when the β-process starts, and the dashed lines shows the time the α-process starts.

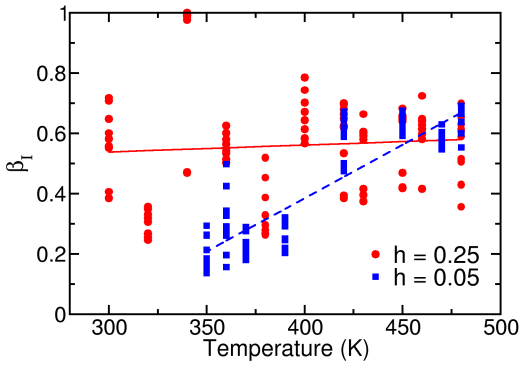

Fig. 6 The stretched exponential parameter, β_I, obtained from the fits of the KWW model to $I(Q,t)$ for $h = 0.05$ (blue solid squares) and $h = 0.25$ (red solid circles) g_{water}/g_{lignin}. At each temperature, Q-values are between 0.2 and 2.0 Å^{-1} range. The lines represent the linear fit to β_I.

the α relaxation regime. The α process is the long-time relaxation that involves collective motions of monomers, found when lignin is liquid-like above T_g. At temperatures below T_g, the β relaxation is the dominant process (Fig. 4a).

Time range of β relaxation

Although the β relaxation is separated from the α (main) relaxation at long times, the two processes are mixed at short times at $T > T_g$. The time range of the β process can be determined by considering that its ISF is given by[49]

$$I_\beta(Q,t) = f^p(Q) + C(Q)G(t), \tag{4}$$

where $f^p(Q)$ is the value of the plateau in $I(Q,t)$ before the α process (See Fig. 4), $G(t)$ represents the temperature and time dependence of $I_\beta(Q,t)$, and $C(Q)$ is a Q-dependent amplitude. The main assumption behind Eq. (4) is that the time dependence of $I(Q,t)$ is contained in $G(t)$ which is independent of Q. This assumption reflects confined motions, whose relaxation is Q-independent. The starting times of the β and α relaxation processes (t_β and t_α, re-

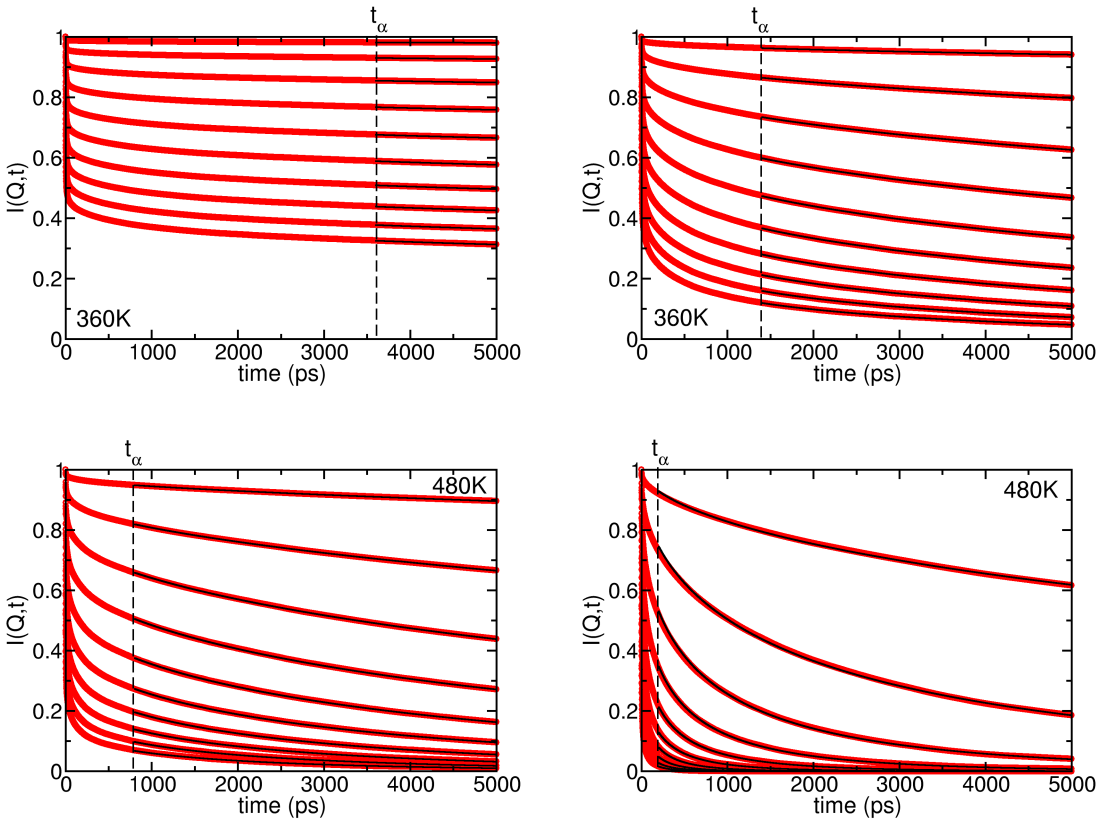

Fig. 7 For (LHS) $h = 0.05$ and (RHS) $h = 0.25$ g_{water}/g_{lignin}, the incoherent intermediate scattering function $I(Q,t)$ for lignin at 360 and 480 K calculated from the second half of a 150-ns MD simulation (red open circles). The black solid lines are the fits of $I_{KWW}(Q,t)$ to $I(Q,t)$ with Q-independent β_I. t_α (black dashed line) represents the starting time of the α process. From top to bottom the Q values are 0.2, 0.4, 0.6, 0.8, 1.0, 1.2, 1.4, 1.6, 1.8 and 2 Å^{-1}.

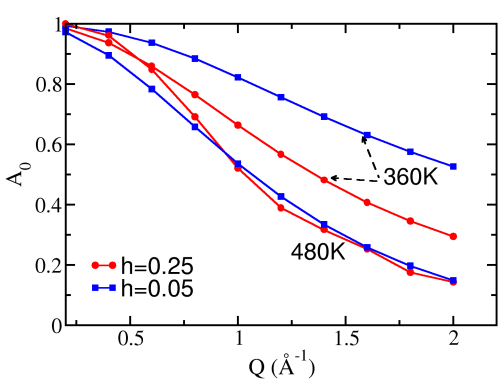

Fig. 8 The Debye Waller factor A_0 obtained from the fits of the KWW model to $I(Q,t)$ for $h = 0.05$ (blue solid squares) and $h = 0.25$ (red solid circles) g_{water}/g_{lignin}.

spectively) in the $I(Q,t)$ were determined here as the slowest and longest times t for which the quantity $R(Q,t)$ is independent of Q, consistent with Eq. (5) (Fig. 5) :

$$R(Q,t) = \frac{I(Q,t) - I(Q,t')}{I(Q,t'') - I(Q,t')} = \frac{G(t) - G(t')}{G(t'') - G(t')} = R(t), \qquad (5)$$

$t' = 100$ and $t'' = 20$ ps are two times in β relaxation regime.

$R(Q,t)$ is independent of Q in a window in time ($t_\beta < t < t_\alpha$) that determines the β relaxation regime, in which $I(Q,t) = I_\beta(Q,t)$. Both t_α and t_β depend on hydration and temperature (Fig. 5). t_β varies between $1-3$ and $1-10$ ps time ranges for 5% and 25% hydrated samples, respectively. t_α was found to decrease with temperature and hydration. For example, t_α is 3.8 ns at 360 K and 0.8 ns at 480 K for the 5% hydrated sample, but 0.8 ns at 360 K and at 0.2 ns at 480 K for the 25% hydrated sample.

Relaxation Time

After determining t_α for all temperatures, the Kohlrausch-Williams-Watts (KWW) stretched exponential function[51] was fitted to the ISF in the α relaxation regime ($t > t_\alpha$), see Fig. 7,

$$I_\alpha(Q,t) = I_{KWW}(Q,t) = A_0 exp(-(t/\tau)^{\beta_I}). \qquad (6)$$

The KWW model includes three fitting parameters: β_I is the stretched exponential parameter ($0 < \beta_I < 1$) that describes the deviation of $I(Q,t)$ from a single exponential function; τ is

the relaxation time, and A_0 is the Debye-Waller factor, $A_0 = exp(-Q^2\langle r^2\rangle/6)$ that defines the first fast decay of $I(Q,t)$. To determine τ, in a preliminary step, τ, β_I and A_0 were all taken as free parameters (see preliminary fits in Fig. S-4 in SI). The best fit values of β_I are found to be dependent on Q for both hydration levels (Fig. 6), with the 5% hydrated sample exhibiting a stronger temperature dependence.

In what follows, to obtain a smooth $Q-$ and temperature-dependence of τ and A_0, a linear fit was applied to β_I fixing it to a constant (Q-independent) value for each temperature (solid lines in Fig. 6). Overall, the fit of the KWW function to the α relaxation time region is excellent for both hydration levels (Fig. 7, S-5 and S-6 in the S.I.). Parameters A_0 and τ are found to depend on temperature and Q. A_0 decreases with increasing Q and temperature (Fig. 8). At 480 K, both samples are above their T_g and have similar A_0. At 360 K, the 5% hydrated sample is below its T_g and thus has larger A_0. The behaviour of τ is discussed below.

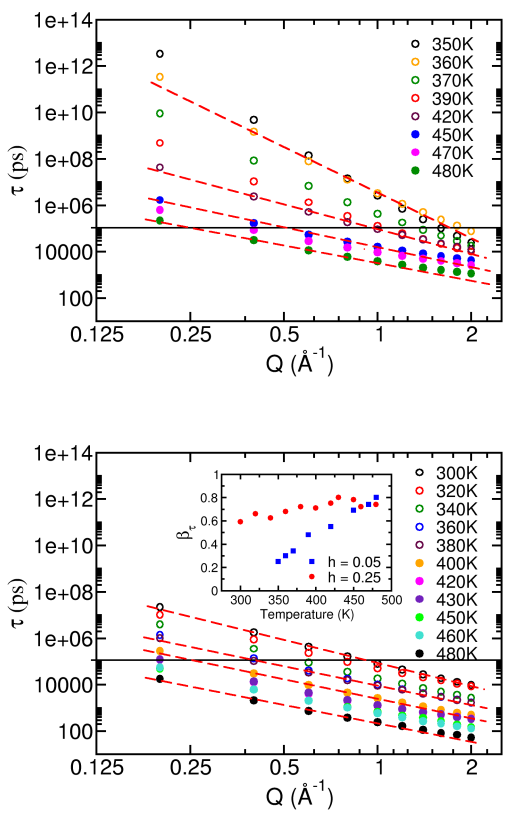

Fig. 9 The relaxation time τ in the α-process versus Q. The dashed lines show the fit of the power law $\tau = Q^{-2/\beta_\tau}$ for (Top) $h = 0.05$ and (Bottom) $h = 0.25$ g_{water}/g_{lignin}. The inset graph on RHS shows the β_τ parameter.

Q-dependence of the relaxation time

The relaxation times τ obtained from the fits in Fig. 7 follow a Q-dependent power law for all temperatures,

$$\tau \simeq Q^{-2/\beta_\tau} \tag{7}$$

indicative of subdiffusion (Fig. 9)[48,52–56]. Similar to β_I, the parameter β_τ depends strongly on temperature for the 5% hydrated sample only (inset Fig. 9). At a given temperature, τ is longer for low hydration, indicating that the dynamics of lignin becomes slower with decreasing hydration (Fig. 9). Thus, for 5% hydrated sample, a longer time is required to observe the large-scale subdiffusion process than the 25% hydrated sample.

For both hydration levels, τ obeys the power law for a limited range : $Q < Q_{max}$. Q_{max} decreases with increasing temperature and hydration. For example, τ obeys the power law up to $Q = 2$ Å^{-1} at 420 K and up to $Q = 1.2$ Å^{-1} at 480 K for the 5% hydrated sample, but diverges from the power law at $Q_{max} = 1.4$ for Å^{-1} at 400 K for the 25% hydrated sample. The breakdown of the power-law at large Q indicates that the α-relaxation is sub-diffusive only above a minimum characteristic length scale $R_{min} = 2\pi/Q_{max}$. $R_{min} \sim 3.1$ Å at 420 K for the 5% hydrated sample and $R_{min} \sim 4.5$ Å at 400 K for the 25% hydrated sample. Thus, R_{min} increases with hydration.

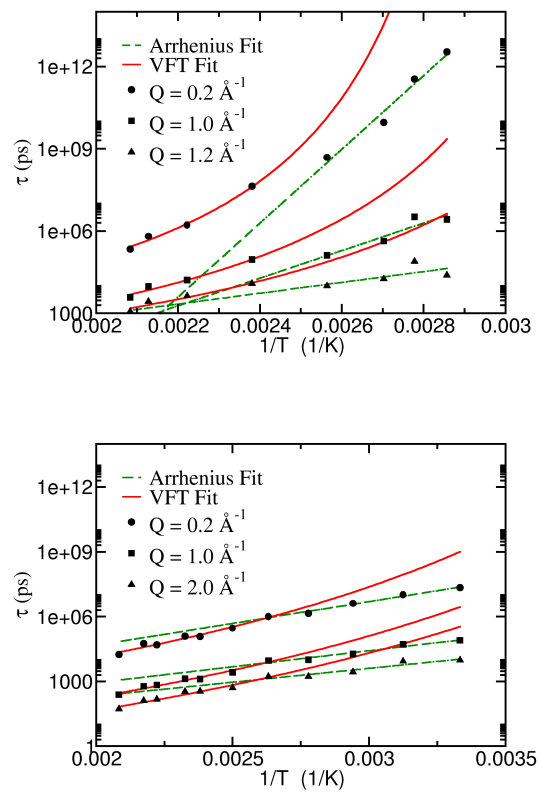

Fig. 10 Relaxation time versus temperature. The solid lines represent the fit of the VFT function, $\tau = \tau_0 \exp(A/T)$, to τ, and the dashed line the fit of the Arrhenius function, $\tau = \tau_0 \exp(B/(T - T_{VF}))$, to τ for (Top) $h = 0.05$ and (Bottom) $h = 0.25$ g_{water}/g_{lignin}.

The temperature dependece of the relaxation time

The temperature dependence of the relaxation time was found to obey two regimes (Fig. 10 and S-7). At low temperatures (in which the β process dominates), τ decreases exponentially with

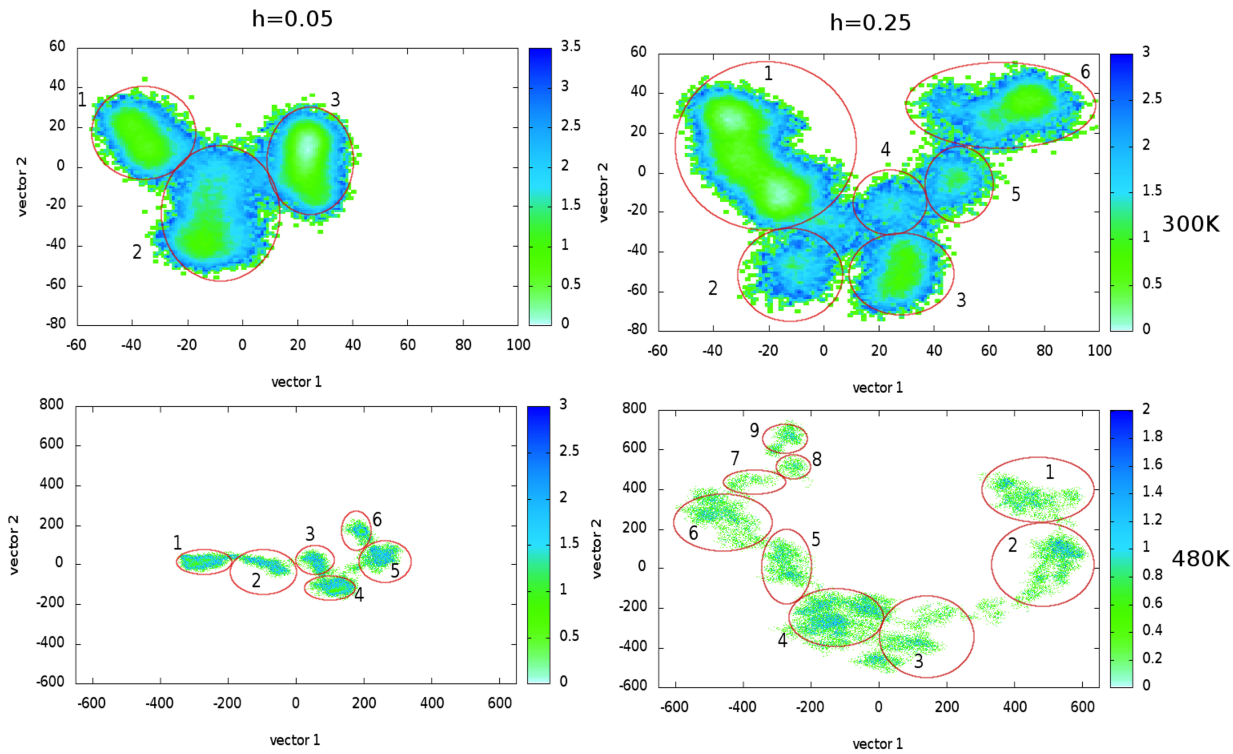

Fig. 11 The projection of the lignin trajectory onto v_1 (first principal component) and v_2 (second principal component) at (top) 300 and (bottom) 480 K for (LHS) $h = 0.05$ and (RHS) $h = 0.25$ g_{water}/g_{lignin}.

temperature, in an Arrhenius temperature dependence,

$$\tau = \tau_0 exp(A/T), \tag{8}$$

where $A = E/k_B$, E is the activation energy, k_B is the Boltzmann constant, T is the temperature, and τ_0 a prefactor[57]. At high temperatures, (in which the α process dominates), the temperature dependence of the relaxation time was found to be non-Arrhenius, described by the Vogel-Fulcher-Tamman (VFT) equation

$$\tau = \tau_0 exp(B/(T - T_{VF})), \tag{9}$$

where B is a material dependent constant and T_{VF} is the VFT temperature.

The Arrhenius and VFT functions were fitted to $\tau(T)$ for ten Q-values, but only $Q = 0.2$, 1.0 and 2.0 Å^{-1} are shown in Fig. 10 (fitting parameter in Fig. S-8 and S-9). Fits for other Q values can be found in Figs. S-7. τ changes from an Arrhenius to a non-Arrhenius temperature dependence at $T \sim 410$ K for the 5% hydrated sample and at $T \sim 350$ K for the 25% hydrated sample. The transition from Arrhenius to non-Arrhenius behaviour in τ is associated with the glass transition. T_g is thus found to be around 420 and 350 K for 5% and 25% hydration, respectively.

Energy Landscape

To analyze the configurational space explored by the molecules in 75 ns of simulation, we projected all atomic displacements on the first two PCs (Fig. 11). The configurational space is considerably more restricted at 300 K, an indication of the localization of lignin atoms. The configurational space is roughly divided into local energy basins, labeled with ellipses in Fig. 11. Time series of the minima visited are ploted in Fig. S-10. The transitions between well-defined minima at 300 K are compatible with the Arrhenius behaviour. At 480K, lignin molecules are not trapped in single minima for long times due to the lower energy barriers. Rather, the dynamical properties arise from the activation of long-distance sub-diffusion well described in terms of a multi-minima energy landscape and consistent with the non-Arrhenius behaviour.

Mean Square Displacement

We also analysed the mean square dispacement (MSD) (Eq. (2)) of non-exchangeable hydrogen atoms in lignin (Fig. 12). At times longer than 1 ns, the MSD increases with time, corresponding to the α-relaxation. A power law, $\sim t^{\beta_m}$ was fitted to MSD data at $t > 1$ ns to determine the exponent β_m, which provides information about the subdiffusive dynamics of lignin. β_m is small for $T < T_g$ (e.g., $\beta_m = 0.19$ at 350 K for $h = 0.05$ and 0.26 at 300 K for $h = 0.25$ g_{water}/g_{lignin}). This indeed indicates that lignin is glassy and its dynamics is slow at $T < T_g$ for both hydration levels. For

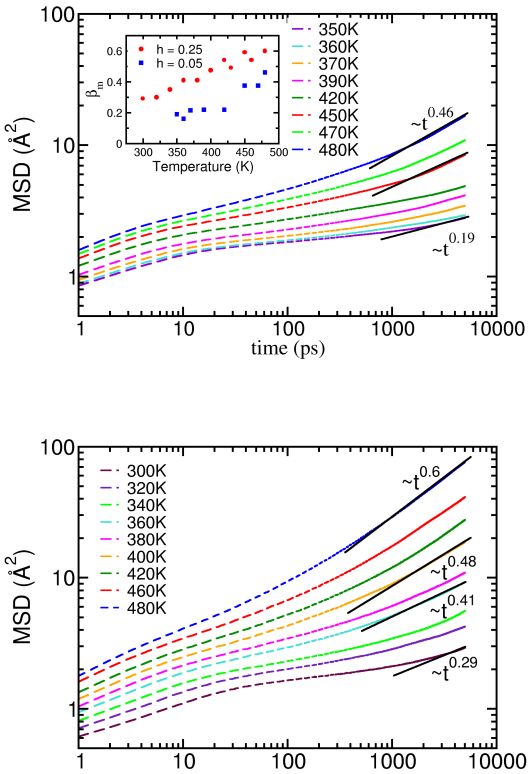

Fig. 12 Mean square displacement of non-exchangeable hydrogen atoms in lignin versus time for (Top) h=0.05 g_{water}/g_{lignin} and (Bottom) h=0.25 g_{water}/g_{lignin}. The inset graph on the top frame shows the β_m parameter obtained from the $\sim t^{\beta_m}$ fit to MSD data.

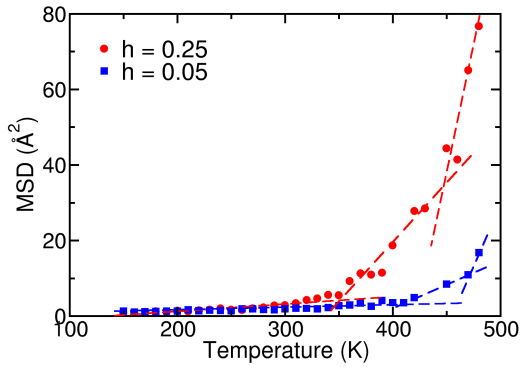

Fig. 13 MSD at 5 ns versus temperature for $h = 0.05$ (blue solid squares) and $h = 0.25$ (red solid circles) g_{water}/g_{lignin}. The dashed lines are guides to the eye.

$T > T_g$, we observe that β_m increases and reaches 0.5 and 0.6 for $h = 0.05$ and $h = 0.25$ g_{water}/g_{lignin}, respectively. The temperature dependence of the β_m was found to be different from that of β_I and β_τ. β_m varies more with temperature for 25% hydrated sample. This difference could arise from the contribution of atoms other than non-exchangeable H to the $I(Q,t)$.

The MSD is different below and above certain temperatures, for both hydration levels. To show this more clearly, the MSD at 5 ns is plotted versus temperature (Fig. 13). The slope of the MSD increases sharply at 420 and 350 K for the 5% and 25% hydrated samples, respectively. This dramatic change in the MSD corresponds to the glass transition, and is consistent with the glass transition temperature observed in Figs. 10 and 12. For both hydration level, a second tansition is observed at 460 K for 5% hydrated sample and at 440 K for 25% hydrated sample. This transition could be arise from a dynamical transition (like protein)[58] or the MSD could increase exponentially above T_g[59,60].

Discussion and Conclusions

Lignin is the second most abundant source of carbon on earth and is important in the production of biofuels and other biomaterials such as carbon fiber and plastics. During thermal pretreatment of plant biomass, lignin becomes softer at temperatures higher than its glass transition temperature due to activated segmental motions. Hence, the temperature dependence of the dynamics of lignin has industrial importance.

Using molecular dynamic simulation, we characterized the temperature and hydration dependence of lignin dynamics. Below T_g, lignin exhibits mainly internal and localized motions. Above T_g segmental motions, which involve about 3-5 monomeric units, dominate and lead to enhanced chain mobility. The segmental motions are subdifusive, *i.e.* their long-range motion is slower than unobstructed Fickian diffusion. We calculated three parameters that quantify the extent of subdiffusion, the higher these parameters are the lower the extent of subdiffusion. The first parameter is β_I, the exponent that determines the decay of the intermediate scattering function (Eq. 6), the second β_τ that determines the power-law Q-dependence of the relaxation time, and the third is β_m, that determines the time-dependence of the atomic mean square displacements. As expected (see S.I. text), all three exponents are found to have similar values and to display similar behavior: they increase with temperature, and this increase is more significant for high hydration.

Lignin is a complex macromolecule that does not have a regular/repeating polymeric primary structure. Additionally, lignin molecules in plants are believed to be highly heterogeneous: having similar average chemical compositions, but different primary sequences[61,62]. Despite this heterogeneity, the temperature (and wave-vector) dependence of the lignin relaxation time was found here to follow the same broad trends as chemically simpler and more homogeneous homopolymers: switching from Arrhenius to non-Arrhenius when the temperature is increased above T_g. However, the underlying energy landscape of lignin is more complex than what would be inferred by a simplistic interpretation of $\tau(T)$. Formally, Arrhenius behavior is expected for a system that transitions between energy minima separated by equal barriers. This is clearly not the case for lignin, which displays multiple minima of varying depth and, nonetheless, still displays an Arrhenius-type temperature dependence.

It is found that hydration and temperature affect lignin dynam-

ics in similar ways. Specifically, increasing either T or h leads to the α process starting earlier (smaller time t_α) and increases the lengthscale above which subdiffusion is observed (Q_{max} decreases). This equivalence of hydration and temperature in enhancing lignin dynamics may be useful when devising strategies to process biomass at lower temperatures and reduced costs.

Acknowledgements

This research was supported by the Genomic Science Program, Office of Biological and Environmental Research, U.S. Department of Energy (DOE), under Contract FWP ERKP752. This research used resources of the National Energy Research Scientific Computing Center, a DOE Office of Science User Facility supported by the Office of Science of the U. S. Department of Energy under Contract No. DE-AC02-05CH11231. Oak Ridge National Laboratory is managed by UT-Battelle, LLC, for DOE under Contract DE-AC05-00OR22725.

Notes and references

1 H. C. Liu, A.-T. Chlen, B. A. Newcomb, Y. Liu and S. Kumar, *ACS Substainable Chem. Eng.*, 2015, **3**, 1943–1954.

2 J. F. Kadla, S. Kubo, R. A. Venditti, R. D. Gilbert and W. Compere, A. L. Griffith, *Carbon*, 2002, **40**, 2013–2920.

3 S. Wang, Y. Li, H. Xiang, Z. Zhou, T. Chang and M. Zhu, *Comp. Sci. Tech.*, 2015, **119**, 20–25.

4 Q. Sun, R. Khunsupat, K. Akato, J. Tao, N. LabbÃĺ, N. C. Gallego, J. J. Bozell, T. G. Rials, G. A. Tuskan, T. J. Tschaplinski, A. K. Naskar, Y. Puf and A. J. Ragauskas, *Green Chemistry*, 2016.

5 C. Somerville, H. Youngs, C. Taylor, S. C. Davis and S. P. Long, *Science*, 2010, **329**, 790–792.

6 H. Jorgensen, J. B. Kristensen and C. Felby, *Biofuels, Bioprod. Biorefin.*, 2007, **1**, 119–134.

7 S.-Y. Ding, Y.-S. Liu, Y. Zeng, M. E. Himmel, J. O. Baker and E. A. Bayer, *Science*, 2012, **338**, 1055–1060.

8 D. A. Baker, N. C. Gallego and F. S. Baker, *J. Appl. Polym. Sci.*, 2012, **124**, 227–234.

9 S. Kubo and J. F. Kadla, *Macromolecules*, 2004, **37**, 6904–6911.

10 S. L. Hilburg, A. N. Elder, H. Chung, R. L. Ferebee, M. R. Bockstaller and N. R. W. hburn, *Polymer*, 2014, **55**, 995 – 1003.

11 M. H. Sipponen, M. Smyth, T. Leskinen, L.-S. Johansson and M. Osterberg, *Green Chem.*, 2017, **19**, 5831–5840.

12 B. S. Donohoe, S. R. Decker, M. P. Tucker, M. E. Himmel and T. B. Vinzant, *Biotechnol. Bioeng.*, 2008, **101**, 913–925.

13 S. P. S. Chundawat, B. S. Donohoe, L. da Costa Sousa, T. Elder, U. P. Agarwal, F. Lu, J. Ralph, M. E. Himmel, V. Balan and B. E. Dale, *Energy Environ. Sci.*, 2011, **4**, 973–984.

14 X. Gao, R. Kumar, S. Singh, B. A. Simmons, V. Balan, B. E. Dale and C. E. Wyman, *Biotechnol. Biofuels*, 2014, **7**, year.

15 N. Lou, Y. Wang, X. Li, H. Li, P. Wang, C. Wesdemiotis, A. P. Sokolov, and H. Xiong, *Macromolecules*, 2013, **46**, 3160.

16 V. N. Novikov and A. P. Sokolov, *Phys. Rev. E*, 2003, **67**, 031507.

17 A. Tejado, C. Pena, J. Labidi, J. M. Echeverria and I. Mondragon, *Bioresource technology*, 2007, **98**, 1655.

18 D. Feldman, D. Banu, J. Campanelly and H. Zhu, *J. App. Poly. Sci.*, 2001, **81**, 861.

19 J. Han, R. H. Gee and R. H. Boyd, *Macromolecules*, 1994, **27**, 7781.

20 M. Li, X. Y. Liu and Y. Gu, *Europhys. Lett.*, 2009, **3**, 665.

21 D. Rigby and R.-J. Roe, *J. Chem. Phys.*, 1987, **12**, 7285.

22 W. G. Glasser and R. K. Jain, *Holzforschung*, 1993, **47**, 225.

23 J. Lisperguer, P. Perez and S. Urizari, *J. Chil. Chem. Soc.*, 2009, **54**, 460.

24 H. Hatakeyama, Y. Tsujimoto, M. Ja Zarubin, S. M. Krutov and T. Hatakeyama, *J. Therm. Anal. Cal.*, 2010, **101**, 289–295.

25 A. M. A. Nada, H. A. Yousef and S. E. Gohary, *J. Therm. Anal. Cal.*, 2002, **68**, 265.

26 J. Bouajila, P. Dole, C. Joly and A. Limare, *J. App. Poly. Sci.*, 2006, **102**, 1445.

27 S. Khodadadi and A. P. Sokolov, *Soft Matter*, 2015, **11**, 4984–4998.

28 K. F. Freed, *J. Chem. Phys.*, 2015, **143**, 051102.

29 W. S. Xu and K. F. Freed, *J. Chem. Phys.*, 2014, **141**, 044909.

30 J. Dudowicz, K. F. Freed and J. F. Douglas, *J. Chem. Phys.*, 2006, **124**, 064901.

31 J. Dudowicz, J. F. Douglas and K. F. Freed, *J. Chem. Phys.*, 2014, **141**, 234903.

32 J. Dudowicz, J. F. Douglas and K. F. Freed, *J. Chem. Phys.*, 2014, **140**, 244905.

33 K. Chen and K. S. Schweizer, *J. Chem. Phys.*, 2007, **126**, 014904.

34 A. P. Sokolov, V. N. Novikov and Y. Ding, *J. Phys. Condens. Mat.*, 2007, **19**, 205116.

35 K. Kunal, C. G. Robertson, S. Pawlus, S. F. Hahn and A. P. Sokolov, *Macromolecules*, 2008, **41**, 7232–7238.

36 F. Chen, Y. Tobimatsu, D. Havkin-Frenkel, R. A. Dixon and J. Ralph, *Proc. Nat. Acad. Sci. U.S.A.*, 2012, **109**, 1772.

37 J. C. Philips, R. Braun, W. Wang, J. Gumbart, E. Tajkhorshid, E. Villa, C. Chipot, R. D. Skeel, L. Kale and K. Schulten, *J. Comp. Chem.*, 2005, **26**, 1781.

38 W. L. Jorgensen, J. Chandrasekhar, J. D. Madura, R. W. Impey and M. L. Pastor, *J. Chem. Phys.*, 1983, **79**, 926.

39 L. Petridis and J. C. Smith, *J. Comp. Chem.*, 2009, **30**, 457.

40 U. Essmann, L. Perera, M. L. Berkowitz, T. Darden, H. Lee and L. G. Pedersen, *J. Chem. Phys.*, 1995, **103**, 8577.

41 S. E. Feller, Y. Zhang and R. W. Pastor, *J. Chem. Phys.*, 1995, **103**, 4613.

42 W. G. Hoover, *Phys. Rev. A*, 1985, **31**, 1695.

43 B. Lindner and J. C. Smith, *Comp. Phys. Com.*, 2012, **183**, 1491.

44 K. Pearson, *Philo. Mag. J. Sci.*, 1901, **2**, 559.

45 K. Pearson, *J. Educ. Psychol.*, 1933, **24**, 417–441, 498–520.

46 A. Arbe, J. Colmenero, F. Alvarez, M. Monkenbusch, D. Richter, B. Farago and B. Frick, *Phys. Rev. E*, 2003, **67**, 051802.

47 A. Naroz, F. Alvarez, A. Arbe, J. Colmenero, D. Richter and B. Farago, *J. Chem. Phys.*, 2004, **121**, 3282.

48 J. Colmenero, F. Alvarez and A. Arbe, *Phys. Rev. E*, 2002, **65**, 041804.

49 K. Binder, J. Baschnagel and W. Paul, *Proc. Polym. Sci.*, 2003, **28**, 115.

50 D. Vural, C. Gainaru, H. O'Neill, Y. Pu, M. D. Micholas Dean Smith, J. M. Parks, S. V. Pingali, E. Mamontov, B. H. Davison, A. P. Sokolov, A. J. Ragauskas, J. C. Smith and L. Petridis, *Green Chemistry*, 2018, **20**, 1602–1611.

51 S. H. Chung and J. R. Stevens, *Am. J. Phys.*, 1991, **59**, 1024.

52 J. Colmenero, A. Alegria and A. Arbe, *Phys. Rev. Lett.*, 1992, **69**, 478.

53 J. Colmenero, A. Arbe and A. Alegria, *J. Non-Cryst. Solids*, 1994, **172-174**, 126–137.

54 A. Arbe, J. Colmenero, M. Monkenbusch and D. Richter, *Phys. Rev. Lett.*, 1998, **81**, 590.

55 J. Colmenero, F. Alvarez, Y. Khairy and A. Arbe, *J. Chem. Phys.*, 2013, **139**, 044906.

56 J. Colmenero, F. Alvarez and A. Arbe, *EPJ Web of Conferences*, 2015, **83**, 01001.

57 H. Lu and W. M. Huang, *Smart Materials and Structures*, 2013, **22**, 105021.

58 K. L. Ngai, S. Capaccioli and A. Paciaroni, *J. Chem. Phys.*, 2013, **138**, 235102.

59 B. Frick, C. Alba-Simionesco, G. Dosseh, C. Le Quellec, A. J. Moreno, J. Colmenero, A. Schonhals, R. Zorn, K. Chrissopoulou, S. H. Anastasiadis and K. Dalnoki-Veress, *J. Non-Cryst. Solids*, 2005, **351**, 2657–2667.

60 C. M. Roland and K. L. Ngai, *J. Chem. Phys.*, 1996, **104**, 2967.

61 V. Vanholme, B. Demedts, K. Morreel, J. Ralph and Boerjan, *Plant Physiology*, 2010, **153**, 895–905.
62 L. B. Davin and N. G. Lewis, *Current Opinion in Biotechnology*, 2005, **16**, 407–415.